COPI coat assembly occurs on liquid-disordered domains and the associated membrane deformations are limited by membrane tension

Jean-Baptiste Manneville[a,1], Jean-François Casella[b], Ernesto Ambroggio[a], Pierre Gounon[c], Julien Bertherat[d], Patricia Bassereau[e], Jean Cartaud[f], Bruno Antonny[b,2], and Bruno Goud[a,1,2]

[a]Unité Mixte de Recherche 144, Centre National de la Recherche Scientifique-Institut Curie, 26 rue d'Ulm, 75248 Paris Cedex 05, France; [b]Université de Nice Sophia-Antipolis Centre National de la Recherche Scientifique, Institut de Pharmacologie Moléculaire et Cellulaire, 660 route des lucioles, 06560 Valbonne, France; [f]Institut Jacques Monod, Centre National de la Recherche Scientifique Unité Mixte de Recherche 7592, Universités Denis Diderot-Paris 7 and Pierre et Marie Curie- Paris 6, 2 Place Jussieu, 75251 Paris Cedex 05, France; [c]Université de Nice Sophia-Antipolis, Parc Valrose, 28 avenue Valrose, 06108 Nice Cedex 2, France; [d]Ecole Normale Supérieure, 46 rue d'Ulm, 75005 Paris, France; and [e]Unité Mixte de Recherche 168, Centre National de la Recherche Scientifique-Institut Curie, 26 rue d'Ulm, 75248 Paris Cedex 05, France

Edited by Charles Barlowe, Dartmouth Medical School, and accepted by the Editorial Board September 12, 2008 (received for review July 26, 2008)

Cytoplasmic coat proteins are required for cargo selection and budding of tubulovesicular transport intermediates that shuttle between intracellular compartments. To better understand the physical parameters governing coat assembly and coat-induced membrane deformation, we have reconstituted the Arf1-dependent assembly of the COPI coat on giant unilamellar vesicles by using fluorescently labeled Arf1 and coatomer. Membrane recruitment of Arf1-GTP occurs exclusively on disordered lipid domains and does not induce optically visible membrane deformation. In the presence of Arf1-GTP, coatomer self-assembles into weakly curved coats on membranes under high tension, while it induces extensive membrane deformation at low membrane tension. These deformations appear to have a composition different from the parental membrane because they are protected from phase transition. These findings suggest that the COPI coat is adapted to liquid disordered membrane domains where it could promote lipid sorting and that its mechanical effects can be tuned by membrane tension.

budding | giant unilamellar vesicle | Golgi | intracellular transport | lipid sorting

The COPI coat is involved in retrograde transport from the Golgi apparatus to the endoplasmic reticulum and in intraGolgi transport (1, 2). Assembly of the COPI coat occurs in two steps: i) binding of the small G protein Arf1 to membranes via a myristoyl lipid anchor and a short *N*-terminal amphipathic helix exposed on GTP binding (3) and ii) subsequent recruitment of coatomer, a complex of seven proteins that interacts directly with Arf1-GTP, cargo proteins, and proteins of the p23/p24 family (2, 4–6). How membrane deformation is achieved to form a COPI-coated vesicle remains unclear. In the case of clathrin-coated vesicles, accessory proteins contribute to membrane deformation through the binding of curved domains (BAR) and/or the insertion of amphipathic helices (7). Similarly, COPII vesicle formation is initiated by the membrane deformation activity of Sar1 through its *N*-terminal amphipathic helix, although all COPII components are required to form a 60-nm spherical coated-profile (8, 9). Because Arf1 is closely related to Sar1, Arf1 could display a similar activity. Bidimensional self-assembly of coatomer could also contribute to the budding of small 60-nm diameter COPI-coated vesicles (10), yet coatomer-coated membranes do not always bend in reconstituted systems (see for instance ref. 5). Interaction of proteins of the p23/p24 family with coatomer has been shown to facilitate coatomer assembly and induce a conformational change in coatomer that could lead to COPI-coated vesicle budding (2). However, even in the presence of p23/p24 proteins, a significant fraction of coated membranes are not deformed (5, 6, 11).

Most data supporting the current model for COPI vesicle formation come from reconstituted systems by using either purified Golgi membranes (10), or liposomes of <1 μm in diameter, which are well adapted to electron microscopy and biochemical analysis (5, 6, 11). Here, we have reconstituted the Arf1-dependant assembly of the COPI coat on giant unilamellar vesicles (GUVs). This system is more suitable to study highly dynamic processes such as budding and fission (12). By using optical microscopy, we could assess the effects of membrane tension and of lipid partitioning on the assembly of the COPI coat and on its ability to deform lipid membranes. Our results suggest that the COPI coat is adapted to membranes in the liquid disordered state, that COPI induces lipid sorting, and that COPI-induced membrane deformation occurs below a given threshold in membrane tension.

Results

Sequential Recruitment of Arf1 and Coatomer on Giant Unilamellar Vesicles. Myristoylated Arf1 and coatomer were labeled with green (Arf1-OG) and red (coatomer-TMR) fluorophores, respectively (see supporting information (SI) *Materials and Methods* and Figs. S1*A* and S2*A*). The labeled proteins were shown to be functional by several biochemical means (Fig. S1 *B* and *C* and Fig. S2 *B*). Fluorescence quantification by confocal microscopy showed that Arf1 weakly bound to GUV membranes close to the Golgi composition (13) ('Golgi mix', see *Materials and Methods*) in the presence of GDP. However, the binding was increased approximately 10 times in the presence of GTP (Fig. 1*A*), in agreement with previous results (14). Arf1 binding, which saturates at a concentration of approximately 0.5 μM, reached a maximal level in $\approx$5 min (data not shown), consistent with the binding kinetics of non-fluorescent Arf1 (11). The mobility of Arf1 in GUV membranes was measured by fluorescence recovery (FRAP) experiments (Movie S1, Fig. S3 and Table S1). Arf1-OG recovery curves yielded a diffusion coefficient $D = 4.7 \pm 0.6$ μm^2/s, very similar to the value obtained for a fluorescent lipid in the same conditions ($D = 6.4 \pm 1.4$ μm^2/s). It should be pointed out that Arf1 binding at this

Author contributions: J.-B.M., P.B., B.A., and B.G. designed research; J.-B.M., E.A., P.G., J.B., J.C., and B.A. performed research; J.-F.C. contributed new reagents/analytic tools; J.-B.M. and J.C. analyzed data; and J.-B.M., B.A., and B.G. wrote the paper.

The authors declare no conflict of interest.

This article is a PNAS Direct Submission. C.B. is a guest editor invited by the Editorial Board.

[1]To whom correspondence may be addressed. E-mail: bruno.goud@curie.fr or jean-baptiste.manneville@curie.fr.

[2]B.G. and B.A. contributed equally to this work.

This article contains supporting information online at www.pnas.org/cgi/content/full/0807102105/DCSupplemental.

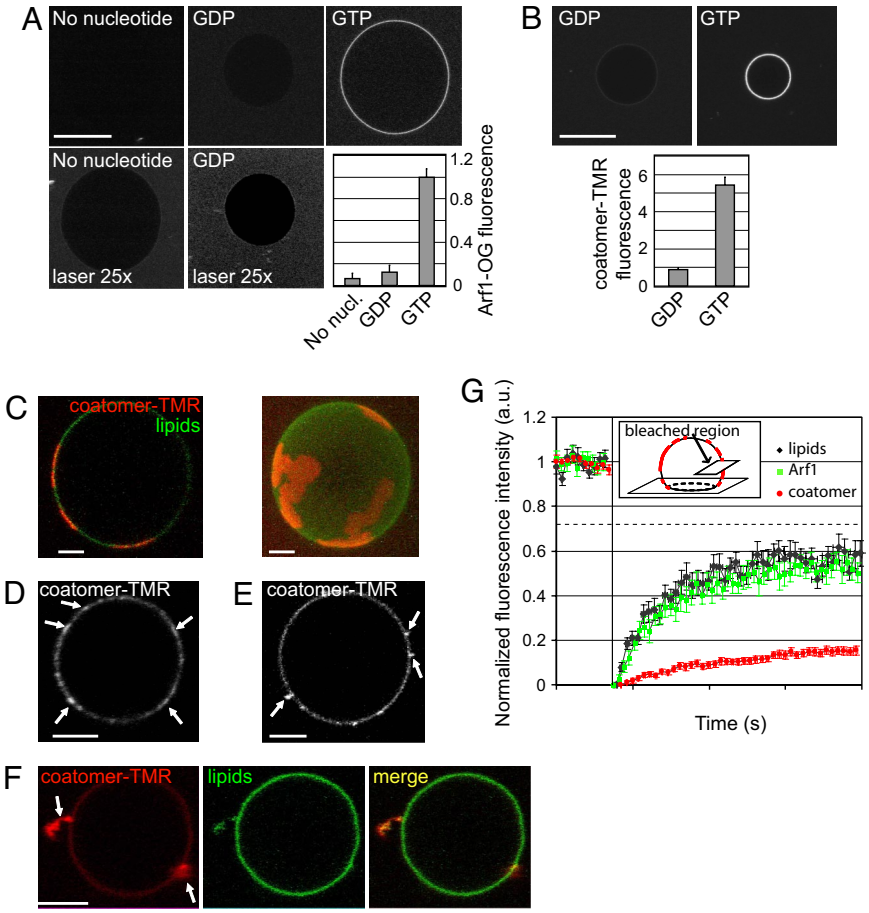

Fig. 1. Sequential recruitment of Arf1 and coatomer on giant unilamellar vesicles (GUVs). (*A*) GUVs were incubated with 0.5 μM Arf1-OG in HKM buffer supplemented with GTP or GDP (0.1 mM). The 'no nucleotide' and 'GDP' images are shown at higher illumination intensity ('laser 25×', lower row). (Scale bar, 20 μm). (*B*) GUVs grown from Golgi mix supplemented with 1.5% (mol/mol) lipopeptide Lp23 were injected in a chamber containing 0.5 μM Arf1 and 0.15 μM coatomer-TMR in HKM buffer and either 0.1 mM GTP or 0.1 mM GDP. In *A* and *B*, quantification of membrane binding of Arf1-OG and of coatomer-TMR was determined from 30 to 35 vesicles in three independent experiments (mean ± SEM). (Scale bar, 20 μm). (*C–F*) Gallery of coatomer-coated GUVs. The experimental conditions were as in *B*. Depending on the GUV, coatomer (red) covers the whole surface (see *B*), forms static domains up to 5 μm in diameter (*C*) or concentrates in small (<1 μm in diameter) dynamic patches (*D*, arrows). Coatomer is also found associated with membrane deformations such as small dynamic budded profiles (arrows in *E*) or tubular profiles (arrows in *F*). The GUV membrane was labeled with 0.5% C5-HPC-BodipyFL (green). All images are confocal sections except the right panel in *C*, which is a 3D projection of a confocal stack. (Scale bars, 5 μm). (*G*) The mobility of coatomer assembled on tensed membranes is reduced compared with free Arf1-GTP and lipids. Averaged FRAP curves showing recovery of coatomer-TMR (red circles, $n = 31$), free Arf1-OG fluorescence (green squares, $n = 31$) and fluorescent lipids (black diamonds, $n = 27$). The photobleached region (see *Inset*) represents ≈20–30% of the total GUV area. The maximal recovery is thus ≈75% (dotted line). Error bars, SEM.

concentration (0.5 μM) did not induce any membrane deformation on GUVs detectable by confocal microscopy.

Next we added fluorescently labeled coatomer. GUVs were grown from Golgi mix supplemented with 1.5% (mol/mol) lipopeptide Lp23 that mimics the cytosolic tail of the Golgi transmembrane protein p23. The presence of Lp23 facilitated coatomer recruitment (Fig. S4) in agreement with previous work (6). In the presence of Arf1 and GTP, coatomer strongly associated with GUV membranes, whereas only weak binding was observed in the presence of GDP (Fig. 1*B*). In ≈50% of the vesicles showing coatomer recruitment, coatomer formed extended (several μm in diameter) domains (Fig. 1*C* and Movie S2) that could cover the entire surface of the vesicle (Fig. 1*B*, 'GTP'), or small (<1 μm in diameter) dynamic patches diffusing on the membrane (Fig. 1*D* and Movie S3). FRAP experiments show that in these structures, coatomer exhibits strongly reduced mobility compared with free Arf1-GTP and lipids (half recovery time $\tau_{1/2} = 14.7 \pm 2.2$ s and mobile fraction $R = 30.6 \pm 1.3\%$ compared with $\tau_{1/2} = 2.7 \pm 0.3$ s, $R = 65.0 \pm 1.4\%$ for free Arf1-GTP and $\tau_{1/2} = 2.3 \pm 0.3$ s, $R = 67.7 \pm 2.0\%$ for lipids) (Fig. 1*G*, Movie S4, and Table S2). These results suggest that the fluorescent patches represent self-assembled flat COPI lattices. Dual visualization of coatomer-TMR and Arf1-OG revealed that Arf1 was concentrated in coatomer patches (Fig. S5).

Membrane Tension Limits Coatomer-Induced Membrane Deformation. In the presence of Arf1-GTP and coatomer, ≈50% of the vesicles displayed optically visible membrane deformations (Fig. 1*E* and Movie S5; Fig. 1*F* and Movie S6). Deformations were enriched in coatomer and in Arf1 (Fig. S5) and were protruding outwards. They remained connected to the vesicle throughout the 2–5-min observation period and no membrane fission was observed. Similar results were obtained by using non-fluorescent coatomer revealed by an antibody against β-COP (Fig. S6). Interestingly, deformations were more frequently observed on fluctuating vesicles, a signature of a low membrane tension, whereas GUVs completely covered with coatomer or exhibiting weakly curved coatomer domains were spherical and appeared under high membrane tension. Membrane tension of GUVs is distributed in the range $\sigma \approx 10^{-6}$-10^{-5} N/m (15). This heterogeneity could explain why approximately half of the vesicles exhibit deformations whereas the other half is not

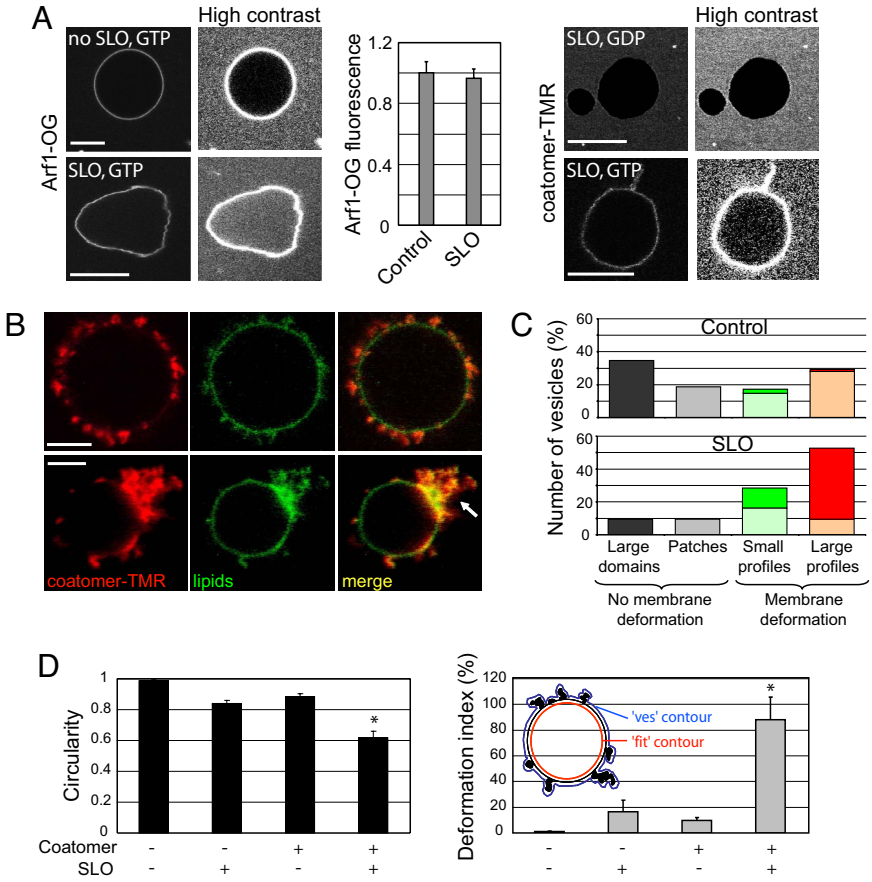

Fig. 2. Low membrane tension facilitates coatomer-induced membrane deformation. (*A*) Streptolysin-O (SLO) was used to decrease membrane tension. Typical images of Arf1-OG (left side) and coatomer-TMR (right image) fluorescence on nontreated control GUVs and on GUVs in the presence of 10 μg/ml SLO are shown. Measurements pooled from 28–38 GUVs in three independent experiments (mean ± SEM) show that Arf1 binds to SLO-permeabilized GUVs to similar levels as in control experiments. High contrast images are provided to show the presence or absence of fluorescent proteins inside GUVs. Arf1-OG but not coatomer-TMR entered SLO-treated GUVs. (Scale bars, 10 μm). (*B*) Golgi mix GUVs with 1.5% (mol/mol) Lp23 were incubated in the presence of Arf1, coatomer-TMR, GTP as in Fig. 1*B* and with 10 μg/ml SLO. The upper images show a GUV with numerous small (0.5–1 μm) and large (> 1 μm) deformation profiles. The lower images show a GUV with a zone of extensive membrane deformation. (Scale bar, 5 μm). (*C*) GUVs at high tension (control, upper graph) or at low tension (SLO, lower graph) were classified into four categories according to the size of the coatomer-coated regions and the extent of membrane deformations (see *SI Materials and Methods*). In the case of deformation profiles, the number of small (0.5–1 μm, N_s) or large (> 1 μm, N_l) profiles on the GUV was counted from a 3D confocal scan. GUVs were scored as displaying a low number of deformations if $N_s \leq 5$ or $N_l \leq 5$ (light green or light red, average numbers of deformations $\bar{N}_s = 2.0 \pm 0.5$, $\bar{N}_l = 1.6 \pm 0.5$ for control GUVs and $\bar{N}_s = 3.6 \pm 0.5$, $\bar{N}_l = 3.0 \pm 0.5$ for SLO-treated GUVs) or a high number of deformations if $N_s > 5$ or $N_l > 5$ (dark green or dark red). Seventy-five vesicles from three independent experiments were scored in each condition. (*D*) Circularity (left image) and the deformation index (right image) were used to quantify membrane deformation (see *SI Materials and Methods* and inset in the right panel). Vesicles (13 to 63) from three independent experiments were scored in each condition (mean ± SEM.). Statistical difference between datasets is indicated (*, $P < 0.001$).

deformed. To further investigate the role of membrane tension, we used the bacterial toxin Streptolysin-O (SLO) that forms approximately 25-nm diameter pores in cholesterol containing membranes (16). Permeabilization of GUVs by SLO leads to a dramatic decrease in membrane tension because of the loss of the constant surface/volume ratio constraint (17). We also tried to decrease membrane tension by increasing the osmotic pressure of the external buffer (18) but the interpretation of the results was ambiguous as this induced severe membrane deformations in the absence of the COPI components. In the presence of 10 μg/ml SLO, GUVs exhibited very strong shape fluctuations, without significant membrane deformation (bottom left side in Fig. 2*A* and Movie S7 and S8). From the maximum amplitude of membrane thermal fluctuations $\langle u(L)\rangle$, we can estimate the membrane tension using $\sigma \propto kT/\langle u(L)\rangle^2 \ln L/a$, where L is the size of the membrane, a is a molecular cut-off length and kT is the thermal energy (19). For a GUV under strong tension, the amplitude of thermal fluctuations is below the optical resolution. Taking $\langle u(L)\rangle < 0.05$ μm for a tense GUV, we find $\sigma_{tense} > 10^{-5}$ N/m, with $L = 10$ μm as the typical GUV diameter, $a = 0.5$ nm the lateral size of a lipid as a molecular cut-off and $kT = 4.3 \times 10^{-21}$ J at 37 °C. For a SLO-permeabilized GUV, the amplitude of fluctuations is typically $\langle u(L)\rangle \approx 1$ μm. At such large amplitudes (10% of the GUV radius) the above formula is not strictly valid, but provides a good estimate of membrane tension in the presence of SLO, yielding a very low value of $\sigma_{SLO} \approx 4 \times 10^{-8}$ N/m. Binding of Arf1 to SLO treated GUVs was found to be similar to control (Fig. 2*A*). However, because we could detect some fluorescence background inside the SLO treated GUVs (see high contrast images in Fig. 2*A*), it is likely that under these conditions Arf1 enters through the SLO pores and binds both to the inner and outer leaflets of the GUV.

After incubation with Arf1-GTP and coatomer, SLO-treated GUVs exhibited extensive membrane deformation. Coatomer, which did not enter through the SLO pores (right side in Fig. 2*A*), concentrated in dynamic profiles, similar to that seen on weakly fluctuating control GUVs (Fig. 1*F*), but the number and/or size of these deformations was greatly enhanced. In some cases, >20–30 profiles per GUV could be observed (Fig. 2*B*, upper image and

Movies S9–S12). Coatomer also induced large extensive membrane deformation (Fig. 2*B*, lower image, arrow). Concomitantly, spherical GUVs fully or partially covered by coatomer (as in Fig. 1*B* or Fig. 1 *C* and *D*) were less frequent than in the absence of SLO. Fig. 2*C* shows a quantification of GUV morphology in the absence and in the presence of SLO (see *SI Materials and Methods*). As in the absence of SLO, no membrane fission was observed.

We quantified the extent of membrane deformation by measuring GUVs circularity and deformation index. Circularity measures the deviation of the vesicle shape form a circular contour, whereas the deformation index measures the excess area incorporated in membrane deformation profiles (see *SI Materials and Methods*). Both parameters indicate strong membrane deformation induced by coatomer at low membrane tension (Fig. 2*D*). Because no fission occurs in the assay, deformations can grow to micrometer sizes. In the presence of pores, we expected the vesicle to shrink completely as the excess area stored in membrane fluctuations was gradually absorbed into coated profiles. We indeed observed such collapsed vesicles (Fig. S7) although they were not typical (Fig. 2*B*). After coatomer binding, the internal contour of the vesicles was in most cases approximately spherical and exhibited weaker shape fluctuations than before incubation with coatomer (compare bottom left images in Fig. 2 *A* with Fig. 2*B*). This suggests a kinetic competition between permeation and coat binding. If coat binding occurs faster than permeation, membrane tension builds up during coat formation and limits membrane deformation. Alternatively, saturation of coatomer binding sites could prevent further membrane deformation.

We also asked whether buds or tubular profiles could form from an initially weakly curved coatomer lattice. We incubated Arf1-GTP and coatomer on GUVs under tension to obtain weakly curved coatomer domains (as in Fig. 1 *C* and *D*) and then injected SLO to decrease membrane tension. Membrane fluctuations appeared only in the regions of the GUVs that were not covered with coatomer, whereas coatomer domains and the underlying membrane did not change shape (Fig. S8 and Movie S13). Quantification shows that the amplitude of membrane fluctuations is twice larger in coatomer-free regions. This suggests that, once assembled, coatomer provides a rigid scaffold that imposes its geometry on the membrane.

The COPI-induced membrane deformations observed in our light microscopy assay are much larger than the 60-nm COPI-coated buds observed by electron microscopy (EM) on Golgi membranes or on small liposomes (5, 6, 10). Because GUVs are brittle objects notoriously difficult to visualize by EM, we developed a protocol based on gentle centrifugation, resin embedding, and thin section EM, allowing ultrastructural characterization of the deformations induced by the COPI coat on GUV membranes at low tension (see *SI Materials and Methods*). The samples were heterogeneous as observed in light microscopy. GUVs showing no or weak coat binding (Fig. S9*A i*) or displaying a few classical 50–60-nm COPI-coated buds (Fig. S9*A ii*) coexisted with extensively deformed coated membranes (Fig. S9*A iii*). These data strongly suggest that the micrometer-sized COPI-induced deformations observed with light microscopy consist of highly convoluted membranes sheets folded into smaller budded and tubular coated profiles. To further investigate by EM the role of membrane tension in COPI-induced deformation, we returned to submicrometer liposomes made by extrusion (5, 6, 11). After incubation with Arf1, GTP, and coatomer, the liposomes were clearly covered by a dense coat but showed variable deformations (Fig. S9*B*). This is illustrated in Fig. 3 where the liposomes were ranked according to the morphology of the budding profiles, from weakly moulded buds to almost circular buds simply connected to the parent liposome by a thin neck. Interestingly, we noticed that when several budding profiles emerged from the same liposome, they exhibited similar shape in terms of curvature and neck size (Fig. 3). These images support a key role for membrane tension in limiting the membrane deformation induced by the COPI coat. Indeed, because the same tension applies all over the liposome surface, each COPI-coated bud must experience the same resistance to deformation as its neighbors.

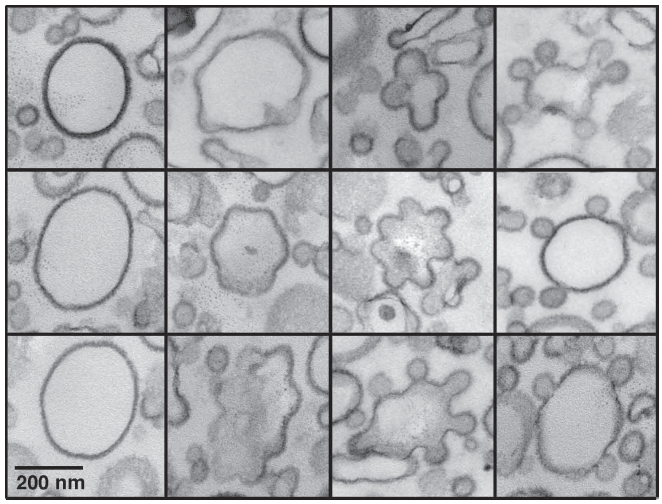

Fig. 3. COPI-coated profiles on submicrometer liposomes. Golgi-mix liposomes with 2 mol% Lp23 were extruded through 0.4 μm polycarbonate filters. After incubation with Arf1, GTP, and coatomer, the sample was fixed with glutaraldehyde and the liposomes were collected by centrifugation and analyzed by thin section EM. The COPI-coated liposomes shown here were selected from the same liposome pellet (see Fig. S9*B*) and were ranked from left to right according to the extent of membrane deformation. (Scale bar, 200 nm)

Interplay Between Lipid Partitioning and COPI Assembly. The composition of the liposomes used in the above experiments approximately mimics a "standard" Golgi composition (13). However, the Golgi apparatus undergoes large changes in lipid composition from the *cis* to the *trans* face. Notably sphingolipids, which were omitted in our standard composition, as well as cholesterol, concentrate at the *trans*-Golgi region where the lipid bilayer becomes also asymmetric. Because COPI vesicles, which arise mostly from the *cis*-Golgi side, have been shown to be partially depleted in sphingomyelin and cholesterol (20), they could contribute to these differences in composition. We thus replaced our standard lipid mixture by GUVs containing more extreme lipid compositions. When GUVs were grown from ternary sphingomyelin/cholesterol/DOPC mixtures exhibiting phase separation between liquid disordered (L_d) and liquid ordered (L_o) domains (21), Arf1-GTP and coatomer partitioned into L_d domains and were strictly excluded from L_o domains (Fig. 4*A* and *B*). Moreover, membrane deformation by coatomer at low membrane tension was observed exclusively in L_d domains (Fig. 4*B*). We concluded that the COPI coat is adapted to membrane domains in the liquid disordered state.

The existence of liquid ordered domains at the Golgi apparatus is a matter of debate. Moreover lipid sorting does not necessary involve preexisting lipid membrane domains; through the extreme curvature imposed on the membrane and by interacting preferentially with some lipid species, protein coats may lead to lipid sorting from an initially homogeneous lipid membrane (21, 22). As a first attempt to test this hypothesis, we used vesicles in the liquid disordered state, but whose membrane composition is close to phase separation, which can be triggered by photoactivation (21). On phase separation, Arf1 segregated into L_d domains and was excluded from L_o domains (Fig. 4*C*) with similar kinetics as L_d lipid markers (data not shown). Strikingly, in the presence of Arf1-GTP and coatomer, phase separation was detected only in noncoated membrane areas (Fig. 4*D*). This result suggests that the COPI coat

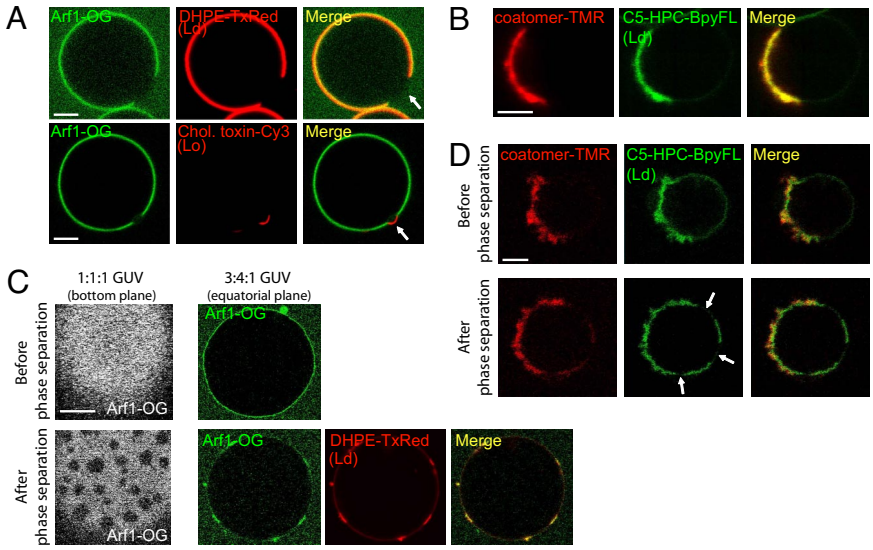

Fig. 4. Arf1 and coatomer partition into liquid disordered (L_d) domains and protect L_d membranes from phase separation. (*A*) GUVs grown from sphingomyelin (BSM)/cholesterol/DOPC (3:1:3) mixtures exhibited phase separation, with μm-sized liquid ordered (L_o) domains surrounded with liquid-disordered (L_d) phase. Arf1-OG (*Left*) localized in the L_d phase (visualized with DHPE-TexasRed) and was excluded from L_o domains (lower image, visualized with cholera toxin-Cy3 and indicated by an arrow). (Scale bar, 5 μm). (*B*) On phase separated 3:2:1 GUVs and in the presence of Arf1-GTP and SLO, coatomer (red, left panel) specifically binds to and deforms L_d domains (visualized with C5-HPC-BodipyFL, green, middle panel). (*C*) Arf1 segregates in L_d domains and is excluded from L_o domains during phase separation. Phase separation was induced from initially homogeneous membranes (upper lane) by photobleaching 1:1:1 (left image) or 3:4:1 (*Right*) GUVs leading to the formation of L_o or L_d domains respectively (lower lane). (*D*) Phase separation occurs only in noncoated regions. Phase separation was induced by photobleaching a 1:1:1 GUV incubated with coatomer-TMR, Arf1, GTP, and SLO. L_o domains (arrows) were detected in the coatomer-free region of the GUV but not in the coatomer-coated area.

locally modifies lipid composition, probably through an enrichment in L_d lipids into coatomer-coated areas, which in turn prevents phase separation.

Discussion

In pioneer studies, it was observed that both Arf1 and coatomer are required for COPI budding from isolated Golgi membranes (1, 10). Our reconstitution of COPI-induced membrane deformation on model giant liposomes is in good agreement with these observations. Membrane deformations are observed only when both Arf1-GTP and coatomer are present. In the absence of coatomer, Arf1-GTP distributes evenly on the GUV surface with no indication of clustering into optically visible membrane deformations. This suggests that the minimal machinery for membrane deformation consists of polymerized Arf1-coatomer complexes.

It has been recently reported that Arf1-GTP deforms membrane sheets or small liposomes into tubules and that this effect depends on key amino acids in the amphipathic *N*-terminal helix as well as in the switch I region (23–25). Because these experiments were performed at a higher protein/lipid ratio than our assay, we suggest that Arf1 contributes to membrane deformation only when it reaches a high surface concentration, that is, upon coat polymerization. In this respect, it should be noted that the *N*-terminal amphipathic helix of Arf1 is shorter and less hydrophobic than the cognate region of Sar1. This reduction in hydrophobicity is probably compensated by the adjacent C14 myristoyl group that inserts in the outer monolayer and should be less perturbing for the membrane than bulky amino acid side chains. This permissive behavior of Arf1 regarding membrane curvature may be key for its multiple functions. Immuno electron microscopy revealed that Arf1 is found on both flat and curved Golgi membranes (10) and, apart from the COPI coat, other Arf1-effector complexes do not necessary require the membrane to be bent (26).

The ability of coatomer to deform membranes strongly depends on membrane tension. The tension of the Golgi apparatus membrane has been estimated to be in the range of $\approx 5 \times 10^{-6}$ N/m (27). This value falls between our estimates for SLO-treated GUVs and for GUVs under tension (see above). Interestingly, the endoplasmic reticulum is thought to have a higher membrane tension than the Golgi apparatus, 1.3×10^{-5} N/m $\geq \sigma_{tense}$ (27). Therefore, the Golgi apparatus membrane should be more prone to deformation than the endoplasmic reticulum membrane. Mechanisms regulating membrane tension of intracellular compartments in vivo, such as interactions with the cytoskeleton, could thus play a key role during membrane trafficking. The effects of other physical parameters such as line tension or bending modulus remain to be tested.

An unexpected finding is that the COPI coat appears to self-assemble on tensed membranes into weakly curved coats, with radii of curvature up to several micrometers. This finding is supported by the observation at the EM level that the COPI coat can cover the entire surface of liposomes of $\approx$0.3 μm in diameter and is confirmed by FRAP experiments, showing that coatomer has strongly reduced mobility compared with lipids and free Arf1-GTP. This suggests that COPI, like clathrin, can form lattices of different curvature. Once assembled into weakly curved coats, the switch to a highly curved coat does not appear to be energetically favored, because reducing membrane tension in our assay did not induce high curvature in initially weakly curved coated membranes. A weakly curved coat may thus have to disassemble completely before self-assembling again in a highly curved conformation (28).

A strong interplay between membrane transport and lipid metabolism occurs at the Golgi apparatus (13, 22, 29). Lipid composition may influence coat machineries, which in turn may contribute to lipid sorting. In our assay we observed that Arf1 and coatomer are completely excluded from model liquid-ordered domains. The extrapolation of this observation to the in vivo situation should be done with caution as the liquid ordered state may exist in vivo only on the luminal side of the *trans*-Golgi network (TGN), thereby remaining inaccessible to Arf1. More intriguing is our observation that COPI coating protects classical liquid disordered membranes from phase transition. This suggests that, through its polymerization and induction of membrane curvature, the COPI coat may con-

tribute to lipid sorting. Our assay should be instrumental to further test this hypothesis because it allows detecting simultaneously membrane deformation and distinct fluorescently labeled lipid species.

Membrane fission is not observed in our assay. A first explanation is that there may be a tradeoff between membrane tension, membrane deformation, and fission (30). Low membrane tension facilitates membrane deformation (our study), whereas high membrane tension may be favorable for fission as suggested by recent works on dynamin (31). Experiments at controlled tension using pipette aspiration should help to resolve this issue. A second explanation is that additional factors may be needed for the fission of COPI coated vesicles. Among the factors that have been invoked are acylCoAs (4), ArfGAP1 and BARS-50 (32) [see however ref. 33] and diacylglycerol (34) but their precise role during fission is unclear. ArfGAP1 hydrolyses GTP in Arf1 and makes the COPI coat quite unstable during membrane deformation (11). With a complete reconstitution including both exchange factors and ArfGAP1 one may recapitulate rounds of GTP binding and hydrolysis and test whether the spatiotemporal control of GTP hydrolysis in COPI coated areas contributes to fission.

Materials and Methods

Details for the preparation and characterization of Arf1-OG and coatomer-TMR can be found in *SI Materials and Methods*.

Reagents. Egg phosphatidylcholine (EPC), liver phosphatidylinositol (LPI), liver phosphatidylethanolamine (LPE), brain phosphatidylserine (BPS), cholesterol, 1,2-dioleoyl-*sn*-glycero-3-phosphocholine (DOPC), brain sphingomyelin (BSM) and GM1 (asialo-GM1-ganglioside) were from Avanti Polar Lipids. Fluorescent lipids (DHPE-TexasRed and C5-HPC-BodipyFL) were from Invitrogen. The B subunit of cholera toxin coupled to Cy3 was a gift from F. Perez (Insitut Curie, Paris, France). Streptolysin-O (SLO) was obtained from S. Bhakdi (Institute of Medical Microbiology and Hygiene, Mainz, Germany). The lipopeptide Lp23 was synthesized as described in ref. 6.

Preparation of Giant Unilamellar Vesicles. GUVs were electroformed in sucrose following a published protocol (35). To avoid any osmotic shock, the osmotic pressure of the sucrose solution was adjusted to match that of the solution containing the proteins. Typically, GUVs were grown in 280 mOsm sucrose for experiments with Arf1 alone, and in 480 mOsm sucrose for experiments with Arf1 and coatomer. 'Golgi mix' is composed of 50% (mol/mol) EPC, 19% LPE, 5% BPS, 10% LPI, and 16% cholesterol. Lipopeptide Lp23 [1.5% (mol/mol)] was added to Golgi mix in coatomer binding experiments. GUVs containing L_d or L_o membrane domains were grown from ternary mixtures of BSM/cholesterol/DOPC as in (21). GM1 (1%) was added in some ternary compositions to visualize L_o domains by binding the B subunit of cholera toxin coupled to the Cy3 fluorophore. GUV membranes were made fluorescent by the addition of 0.5–1% (vol/vol) DHPE-TexasRed or C5-HPC-BodipyFL.

Optical Microscopy. A 5–7-μl observation chamber was made by assembling a coverslip and a glass slide with two parafilm spacers $\approx$1–2 mm apart. To prevent GUV adhesion to the glass, the chamber was incubated with 5 mg/ml casein for 10 min and rinsed twice with HKM buffer (50 mM Hepes, pH 7.2, 120 mM potassium acetate, and 1 mM $MgCl_2$). Proteins in HKM buffer were then injected in the chamber followed by 1–2 μl of GUVs at the same osmotic pressure. GDP to GTP exchange in Arf1-OG was promoted by the addition an excess of GTP (0.1 mM) and by lowering the concentration of free Mg^{2+} to 1 μM by adding 2 mM EDTA. After a 10–15-min incubation the concentration of free Mg^{2+} was raised back to 1 mM by adding 2 mM $MgCl_2$. Because Arf1-OG binding to GUVs saturates at concentrations $>$0.5 μM (data not shown), we used 0.5 μM Arf1 in all fluorescence microscopy experiments. Coatomer was used at 0.15 μM as in (11). Images were taken on a Zeiss LSM510 Meta confocal microscope. Laser powers and detector gains were adjusted in the green and red channels to obtain negligible bleedthrough. Movies shown as *SI Materials and Methods* were taken typically at 1 frame/sec.

Electron Microscopy of COPI-coated Extruded Liposomes. Golgi-mix liposomes (0.1 mM) supplemented with 2 mol% Lp23 obtained by extrusion through 0.4 μm polycarbonate filters were incubated at 37 °C for 10 min with Arf1 (1 μM) and GTP in HKM buffer supplemented with 2 mM EDTA to promote Arf1 activation. Then, 2 mM $MgCl_2$ and 0.3 μM coatomer were added and the sample was further incubated for 6 min. The recruitment of Arf1 and of coatomer was followed by measuring light-scattering at 350 nm of the suspension. The sample was fixed with 2% glutaraldehyde and centrifuged at 100,000 $\times$ *g* for 20 min. The pellet was washed with 0.1M cacodylate buffer and postfixed with 1% osmium tetroxide in the same buffer. The sample was then embedded in epoxy resin and processed for EM observation.

ACKNOWLEDGMENTS. We thank Gerbrand Koster, Frank Perez, Aurélien Roux, and Pierre Sens for stimulating discussions. We thank Joanne Young for critical reading of the manuscript. We thank Mabel San Roman (EM facility Institut Jacques Monod) for assistance with electron microscopy on giant liposomes, the Platforme d'Imagerie Cellulaire et Tissulaire of Institut Curie and the Nikon Imaging Center at the Institut Curie. This work was supported by the Centre National de la Recherche Scientifique, the Institut Curie, and a Grant from the Agence Nationale De La Recherche (ANR) Contract ANR-05-BLANC-0095–01.

1. Rothman JE (1994) Mechanisms of intracellular protein transport. *Nature* 372:55–63.
2. Bethune J, Wieland F, Moelleken J (2006) COPI-mediated transport. *J Membr Biol* 211:65–79.
3. Antonny B, Beraud-Dufour S, Chardin P, Chabre M (1997) N-terminal hydrophobic residues of the G-protein ADP-ribosylation factor-1 insert into membrane phospholipids upon GDP to GTP exchange. *Biochemistry* 36:4675–4684.
4. Ostermann J, *et al.* (1993) Stepwise assembly of functionally active transport vesicles. *Cell* 75:1015–1025.
5. Spang A, Matsuoka K, Hamamoto S, Schekman R, Orci L (1998) Coatomer, Arf1p, and nucleotide are required to bud coat protein complex I-coated vesicles from large synthetic liposomes. *Proc Natl Acad Sci USA* 95:11199–11204.
6. Bremser M, *et al.* (1999) Coupling of coat assembly and vesicle budding to packaging of putative cargo receptors. *Cell* 96:495–506.
7. McMahon HT, Gallop JL (2005) Membrane curvature and mechanisms of dynamic cell membrane remodelling. *Nature* 438:590–596.
8. Lee MC, *et al.* (2005) Sar1p N-terminal helix initiates membrane curvature and completes the fission of a COPII vesicle. *Cell* 122:605–617.
9. Bielli A, *et al.* (2005) Regulation of Sar1 NH2 terminus by GTP binding and hydrolysis promotes membrane deformation to control COPII vesicle fission. *J Cell Biol* 171:919–924.
10. Orci L, Palmer DJ, Amherdt M, Rothman JE (1993) Coated vesicle assembly in the Golgi requires only coatomer and ARF proteins from the cytosol. *Nature* 364:732–734.
11. Bigay J, Gounon P, Robineau S, Antonny B (2003) Lipid packing sensed by ArfGAP1 couples COPI coat disassembly to membrane bilayer curvature. *Nature* 426:563–566.
12. Presley JF, *et al.* (2002) Dissection of COPI and Arf1 dynamics in vivo and role in Golgi membrane transport. *Nature* 417:187–193.
13. van Meer G, Voelker DR, Feigenson GW (2008) Membrane lipids: Where they are and how they behave. *Nat Rev Mol Cell Biol* 9:112–124.
14. Franco M, Chardin P, Chabre M, Paris S (1995) Myristoylation of ADP-ribosylation factor 1 facilitates nucleotide exchange at physiological Mg2+ levels. *J Biol Chem* 270:1337–1341.
15. Solon J, *et al.* (2006) Negative tension induced by lipid uptake. *Phys Rev Lett* 97:098103.
16. Sekiya K, Satoh R, Danbara H, Futaesaku Y (1993) A ring-shaped structure with a crown formed by streptolysin O on the erythrocyte membrane. *J Bacteriol* 175:5953–5961.
17. Koster G, VanDuijn M, Hofs B, Dogterom M (2003) Membrane tube formation from giant vesicles by dynamic association of motor proteins. *Proc Natl Acad Sci USA* 100:15583–15588.
18. Romer W, *et al.* (2007) Shiga toxin induces tubular membrane invaginations for its uptake into cells. *Nature* 450:670–675.
19. Helfrich W (1973) Elastic properties of lipid bilayers: Theory and possible experiments. *Z Naturforsch [C]* 28:693–703.
20. Brugger B, *et al.* (2000) Evidence for segregation of sphingomyelin and cholesterol during formation of COPI-coated vesicles. *J Cell Biol* 151:507–518.
21. Roux A, *et al.* (2005) Role of curvature and phase transition in lipid sorting and fission of membrane tubules. *EMBO J* 24:1537–1545.
22. Holthuis JC, Levine TP (2005) Lipid traffic: Floppy drives and a superhighway. *Nat Rev Mol Cell Biol* 6:209–220.
23. Beck R, *et al.* (2008) Membrane curvature induced by Arf1-GTP is essential for vesicle formation. *Proc Natl Acad Sci USA* 105:11731–11736.
24. Krauss M, *et al.* (2008) Arf1-GTP-induced tubule formation suggests a function of Arf family proteins in curvature acquisition at sites of vesicle budding. *J Biol Chem* 283:27717–27723.
25. Lundmark R, Doherty GJ, Vallis Y, Peter BJ, McMahon HT (2008) Arf family GTP loading is activated by, and generates, positive membrane curvature. *Biochem J* 414:189–194.
26. Drin G, Morello V, Casella JF, Gounon P, Antonny B (2008) Asymmetric tethering of flat and curved lipid membranes by a golgin. *Science* 320:670–673.
27. Upadhyaya A, Sheetz MP (2004) Tension in tubulovesicular networks of Golgi and endoplasmic reticulum membranes. *Biophys J* 86:2923–2928.
28. Harrison SC, Kirchhausen T (1983) Clathrin, cages, and coated vesicles. *Cell* 33:650–652.
29. Patterson GH, *et al.* (2008) Transport through the Golgi apparatus by rapid partitioning within a two-phase membrane system. *Cell* 133:1055–1067.
30. Antonny B (2006) Membrane deformation by protein coats. *Curr Opin Cell Biol* 18:386–394.
31. Roux A, Uyhazi K, Frost A, De Camilli P (2006) GTP-dependent twisting of dynamin implicates constriction and tension in membrane fission. *Nature* 441:528–531.
32. Yang JS, *et al.* (2005) A role for BARS at the fission step of COPI vesicle formation from Golgi membrane. *EMBO J* 24:4133–4143.
33. Gallop JL, Butler PJ, McMahon HT (2005) Endophilin and CtBP/BARS are not acyl transferases in endocytosis or Golgi fission. *Nature* 438:675–678.
34. Fernandez-Ulibarri I, *et al.* (2007) Diacylglycerol Is Required for the Formation of COPI Vesicles in the Golgi-to-ER Transport Pathway. *Mol Biol Cell.*
35. Angelova MI, Soléau S, Méléard P, Faucon JF, Bothorel P (1992) Preparation of giant vesicles by external AC electric fields. Kinetics and applications. *Progr Colloid Polym Sci* 89:127–131.